

Kaolinite based risk assessment of traffic-related pollution for selected historical libraries in Istanbul: Insights from urban topsoils studied by DRIFTS

Ozan Unsalan^{a,*}, Cisem Altunayar-Unsalan^b, Alpaslan H. Kuzucuoglu^c

^aEge University, Faculty of Science, Department of Physics, 35100, Bornova, Izmir, Turkey

^bEge University, Central Research Testing and Analysis Laboratory Research and Application Center, 35100, Bornova, Izmir, Turkey

^cIstanbul Medeniyet University, Faculty of Arts and Humanities, Department of Information and Document Management, 34720, Kadikoy, Istanbul, Turkey

ABSTRACT

This study involves mid infrared (MIR) region (400-4000 cm^{-1}) Diffuse Reflectance Infrared Fourier Transform Spectroscopy (DRIFTS) investigation of urban topsoil samples nearby historical libraries in historic peninsula, Fatih district, Istanbul, Turkey. With DRIFTS, we aimed to detect traffic-driven pollution around these libraries that contain cultural heritage indoors. DRIFTS is a rapid and versatile technique that can be both used in laboratory and in situ soil analysis and it is very sensitive to both organic and mineral soil composition. IR spectral discrimination of topsoil samples collected nearby libraries were rapidly and accurately determined. Another purpose of this work was to investigate the possible sources of pollutants on urban topsoils nearby these historical libraries by their soil mineralogy, mainly based on kaolinite, total recoverable hydrocarbon (TRH), disorder index (DI) and sulfur dioxide (SO_2), as an anthropogenic source, using DRIFTS. To the best of our knowledge, we report the first DRIFTS determination of the various traffic-driven pollution sources absorbed by urban topsoils nearby historical libraries.

*Corresponding author

e-mail: physicistozan@gmail.com

Keywords: Kaolinite, DRIFTS, urban topsoil, historic libraries, pollution, cultural heritage.

1. Introduction

It is very well known that Infrared (IR) spectroscopy is a versatile technique in characterizing soil mineral components and it allows to identify specific peaks stand for vibrations such as O-H, Si-O and Al-O which arise from certain types of minerals thus determine minerals exist in the soil. For example, regarding phyllosilicate identification, absorbance of mineral structural units, mostly hydroxyl, silicate and interlayer and octahedral layer cations are investigated. Hydroxyl O-H stretching and bending occur at $3750\text{-}3400\text{ cm}^{-1}$ and $950\text{-}600\text{ cm}^{-1}$, respectively. Silicate Si-O stretching vibration corresponds to $1200\text{-}700\text{ cm}^{-1}$ and $700\text{-}400\text{ cm}^{-1}$. In addition, interlayer cation vibrations fall into region between $150\text{-}70\text{ cm}^{-1}$ and 2:1 layer silicates contain single O-H stretching band between $3700\text{-}3620\text{ cm}^{-1}$, whereas 1:1 layer silicates absorb two or more stretching bands in this region. In 2:1 layer silicates, isomorphic substitution disrupts crystalline order and causes the single band at 3700 cm^{-1} (Margenot et al., 2017).

Diffuse Reflectance Infrared Fourier Transform Spectroscopy (DRIFTS) is well suited for soil analysis because the spectra can be obtained directly from the samples with minimal sample preparation. Typically only drying and grinding are required, although dilution with KBr is sometimes beneficial. Grinding is best done finely and uniformly across the sample set in order to avoid artifacts that could affect the baseline and peak widths (20 mesh should suffice). Coarser soils trap light more effectively than finer soils, resulting in higher overall absorbance and a shifted baseline (Reeves, 2012). Additionally, mineral bands can be affected by particle size due to variations in specular distortion between small and large silica fragments (Nguyen et al., 1991). Fine grinding can additionally improve spectral quality by homogenizing

soil samples. Similar to transmission analysis of pressed pellets, DRIFTS can be used to analyze soil or sediment samples diluted with KBr (typically 2–10% sample by mass). Quantitative calibrations with soil samples can only be achieved using spectra from “as is” neat samples not diluted with KBr (Janik et al., 1998; Reeves et al., 2001). However, studies on some products including foods (Downey et al., 1997; Kemsley et al., 1996; Reeves, 1994a, 1994b, 2001a, 2001b), forages and soils (Janik et al., 1998) have demonstrated that quantitative analysis using DRIFTS and neat samples can be performed with high accuracy. On the other hand, some studies focused on determination of organic and inorganic carbon by means of Mid IR spectroscopy (Reeves et al., 2002). In order to predict soil pH, soil organic carbon, total nitrogen, exchangeable Al, Ca, Mg, K and soil texture for soil samples, MIR spectroscopy was also performed (Bashagaluke et al., 2015). Soil organic matter (SOM) from two Brazilian soils were investigated in bulk samples and characterized by elemental analyses, DRIFTS and transmission IR spectroscopy. Additionally UV-Vis spectroscopic study was also done on soil samples (Dick et al., 2003).

In the beginnings of 90's, Nguyen et al. (1991) applied DRIFTS in soil studies and they revealed the clay mineralogy and organic matter of the investigated soil samples. In that study, main focus was identification of minerals like quartz, kaolinite, dolomite, illite and montmorillonite. Reference spectra of the pure minerals were compared to the soil spectra and quartz and carbonates were easily identified (Nguyen et al., 1991). It is also important to elucidate humic acid (HA), fulvic acid (FA), composts and peat in soil samples. Characteristic wavenumbers of HA and FA were determined with the aid of DRIFTS and the corresponding band assignments were reported (Niemeyer et al., 1992). Besides, it was pointed out that a decrease in organic carbon (C) is accompanied by a decrease of hydrophobicity as well as soil microbial activity and aggregate stability. That work described hydrophobicity index (HI) as the area of the aliphatic C–H stretching band in the 3000–2800 cm^{-1} spectral region divided by

organic C (Capriel et al., 1995). An earlier work showed that HI is a sensitive quantity to characterize the quality of oil organic matter and it was shown that hydrophobicity of SOM can be determined rapidly by DRIFTS (Capriel, 1997).

In another research conducted by Kaiser et al. (1997), DRIFTS was used for identification of minerals like illite, ferrihydrite, goethite and $\text{Al}(\text{OH})_3$ and they assigned the corresponding absorption bands of dissolved organic matters upon the addition of acidic HA substances. They discussed the alterations of the band intensities and shifts in the spectra in terms of interactions of various functional groups and found that acidic HA substances involve carboxyl groups and aromatic structures. In that work, it was also found that most of the carboxyl groups reacted with metal atoms at the surfaces of $\text{Al}(\text{OH})_3$, ferrihydrite and goethite (Kaiser et al., 1997). Woelki et al. (1997) also studied HA for hydrophobic and hydrophilic fractions and only assigned the types of the functional groups. Salt migration determination investigation was also performed by DRIFTS in the context of preservation of historical monuments and this study was conducted by alkali metal carbonates like Li_2CO_3 , Na_2CO_3 and K_2CO_3 . In that investigation, treated and untreated samples of Burgprepaccher sandstone were investigated and potential harm properties were compared and discussed by absorption intensity using Kubelka-Munk algorithm (Zeine and Grobe, 1997). Machovic and Novak (1998) analysed bitumens isolated from the individual soil horizons of the cambisol samples in Boubin-north spruce stand (Sumava Mountains) and showed the correlation between compositional changes of soil bitumens with increasing soil depth (Machovic and Novak, 1998).

A previous research showed that soils possessing kaolin, gibbsite, goethite, and hematite particles have been found to have a natural capacity to attenuate pollution in aqueous phase (Mohsenipour et al., 2015). That study demonstrated that kaolin can be used for natural scavenger of pollution in the environment. In terms of the relation between soil minerals and

traffic-related pollution, there are still a limited number of studies, yet. One of these studies was on the cadmium (Cd) accumulation on kaolinite and it was found that Cd can be adsorbed across the soil bed (Kim et al., 2003). In a very recent work, researchers investigated the role of the soil-mineralogy in the oral bioaccessibility which has not been extensively studied so far. To investigate bioaccessibility they collected five types of periurban soils and samples were spiked with the same amount of lead-chromates from traffic paint, and subjected to the in vitro Physiological Based Extraction Test (PBET). By this test, they found that Correlation of Pb (lead)-bioaccessible at intestinal conditions is significant with kaolinite (Gonzalez-Grijalva et al., 2019).

More recent evidence showed that DRIFTS is capable of detecting specific organic and inorganic compounds in metal complexes and minerals, thus has been used to predict soil composition and heavy metal contents (Wang et al., 2017). Moreover, among various pollutants such as nitrogen oxides, hydrocarbons, carbon monoxide and carbon dioxide, pollution of the air by sulfur dioxide already exists wherever fossil fuels are burned. At this point, DRIFTS is a promising, rapid and accurate analytical spectroscopic technique for the determination of sulfur dioxide in terms of sulfite in ambient air samples (Verma et al., 2007). In the last few years, major efforts on both determination of soil contamination and total petroleum hydrocarbon concentration were made via DRIFTS by using some key parameters such as area under curves in spectra, regression analysis and intensity ratios of some selected peaks in well-defined ranges in order to build a robust model. In these cutting-edge papers, DRIFTS was thoroughly used and advantage of together with the aid of multiple regression model was taken (Forrester et al., 2013; Hopley et al., 2014; Horta et al., 2015; Ng et al., 2017). An important risk assessment was done by characterization of road dust and minerals such as quartz, muscovite, albite, kaolinite, microcline, Fe-enstatite, graphite and amorphous content and the findings were also associated with health risks (Candeias et al., 2020) and it was highlighted that it is crucial to

identify these minerals and make correlations with traffic related pollutants. Furthermore, a recent study was performed to characterize pollution and identify the source of heavy metals in soils was done using geochemical baseline concentrations (Jiang et al., 2020b) and contamination and ecological and human health risks from different sources of soil heavy metals were evaluated and discussed (Jiang et al., 2020a).

In this context, since vast majority of previous works have only focused on numerous different analytical techniques rather than spectroscopy, there is still a lack of research by spectroscopic techniques in particularly soil research. The purpose of this work was to investigate the possible sources of pollutants on urban topsoils nearby selected historical libraries in Fatih district in Istanbul by their soil mineralogy, mainly based on kaolinite, total recoverable hydrocarbon (TRH), disorder index (DI) and sulfur dioxide (SO₂) as an anthropogenic source using DRIFTS. We also focused on risk assessment for such priceless cultural heritage assets based on our spectroscopic findings. To the best of our knowledge, we report the first DRIFTS investigation on determination of the various sources on urban topsoil samples nearby historical libraries by means of kaolinite, TRH, DI, SO₂ together with the risk assessment.

2. Materials and Methods

2.1. Soil samples

Soil samples were collected from three different parts of the libraries. First; front part of the building (coded “**F**” for spectrum which stands for “**front**” of the building), second; middle part of the library garden (coded “**M**” for spectrum which stands for “**middle**” of the building) and third; backyard of the library garden (coded “**B**” for spectrum which stands for “**backyard**” of the building). Sample weights before and after drying in the microwave oven

were given in Table 1. Weighed soil samples and all samples in the petri dishes after sieving was presented in Fig. 1.



Fig. 1. Weighed soil samples (left) and all samples in the petri dishes after sieving (right).

Table 1. Sample weights before and after drying in the oven.

Sampling sites	Code	Mass (g)	Mass (g)
		(before drying)	(after drying)
Atıf Efendi 1	AF	2.00	1.98
Atıf Efendi 2	AM	2.00	1.99
Atıf Efendi 3	AB	2.00	1.98
Beyazıt 1	BF	2.00	1.97
Beyazıt 2	BM	2.00	1.97
Beyazıt 3	BB	2.00	1.97
Millet 1	MF	2.00	1.97
Millet 2	MM	2.00	1.97
Millet 3	MB	2.00	1.96
Nur-u Osmaniye 1	NF	2.00	1.97
Nur-u Osmaniye 2	NM	2.00	1.98
Nur-u Osmaniye 3	NB	2.00	0.96
Ragıp Paşa 1	RF	2.00	1.95
Ragıp Paşa 2	RM	2.00	1.97
Ragıp Paşa 3	RB	2.00	1.97
Süleymaniye 1	SF	2.00	1.97
Süleymaniye 2	SM	2.00	1.96
Süleymaniye 3	SB	2.00	1.99

2.2. Locations of the collected soil samples combined in Google Earth and Google My Maps

All coordinates (latitudes and longitudes) of the sampling sites were given in Table 2. These coordinates were exported to Microsoft Excel, then imported from Maps Google website as a table and collection spots were plotted based on their location codes and “disorder index” (DI) (between: 0.46 and 0.66), relative intensity of kaolinite peaks observed at 3669 and 3650 cm^{-1} (for details of DI, refer Section 2.3). Google Earth map (Fig. 2) was used to visualise three dimensional (3D) topography of the collection spots. Close-up images of the spots were given in Figs. S1-S6 in Supplementary File. Table 2 also includes selected peak intensity ratios, potential wettability index (PWI) (refer Section 2.3), areas under selected curves and selected Full Width Half Maxima (FWHM) values.

2.3. Potential Wettability Index (PWI) and Disorder Index (DI)

A potential wettability index (PWI) was defined from the ratio of hydrophobic and hydrophilic functional groups in soil organic matter (SOM). It was proposed by Leue et al. (2013) for the first time (Leue et al., 2013). A higher value of PWI means that the SOM has relatively more C–H in comparison to C=O functional groups, and indicates decreased wettability of the surfaces. DRIFTS can be used to obtain IR spectra from intact sample surfaces. DRIFTS were also used to determine this ratio in the SOM (PWI) of intact aggregate coatings by Ellerbrock et al., (2009) and Leue et al., (2013).

A quantitative relation between the relative intensities of the bands at 3669 and 3650 cm^{-1} was defined as the crystallographical order of kaolinite (Cases et al., 1982) and this is called “disorder index” (DI). DI was defined according to previous observations on sedimentary kaolinites (Cases et al., 1982), soil kaolinites (Muller and Bocquier, 1987), and hydrothermal kaolinites (Muller et al., 1990), increases with increasing degree of order.

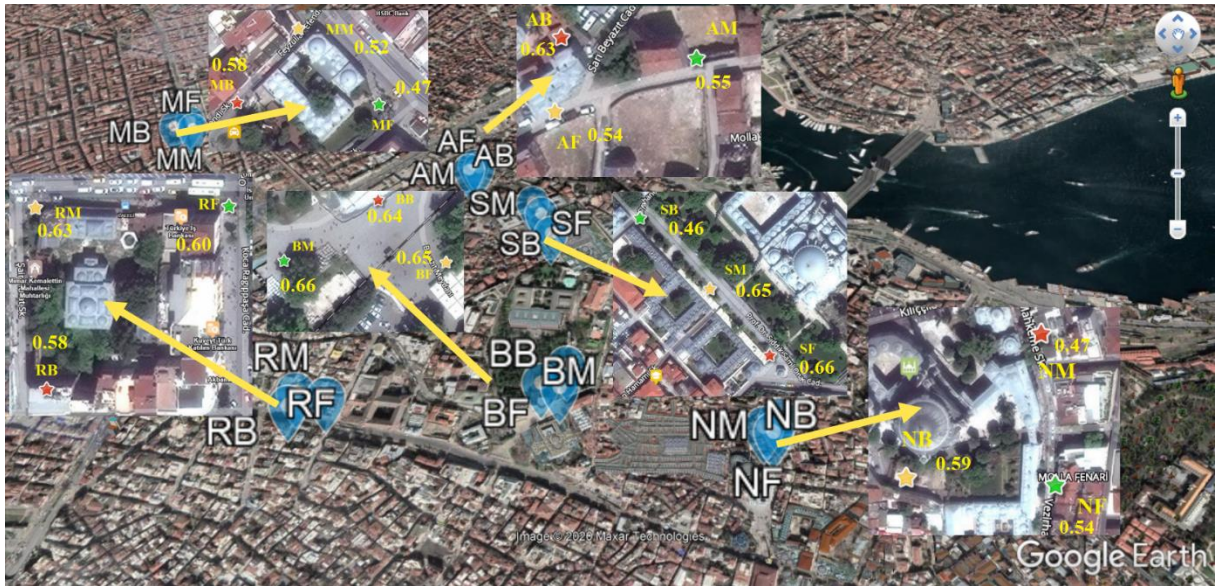


Fig. 2. All locations of the sampling sites nearby historical libraries spotted on Google Earth together with the codes, DI (refer section 2.3) and Total Recoverable Hydrocarbon (TRH) (refer Section 3.1.10) data.

Table 2. Locations of the collected samples together with data for PWI, intensity ratios, DI, areas under selected curves and Full Width at Half Maxima (FWHM) for selected bands.

Location code ^a	Latitude (North)	Longitude (East)	Intensity ratios			PWI ^c	Selected integrated area			FWHM data for selected bands ^d								
			C-H 2924/2873 ^b	C-H 2873/2924	O-H (DI) 3669/3640		C-H Area 2825-3000	1650 Area	1032 Area	2874	2920	2515	2357	1796	1636	1160	810	715
AB	41.017091	28.960206	0.28	3.46	0.63	0.16	1.91	20.13	1.426	31.96	n.d.	33.29	15.77	11.68	57.73	n.d.	n.d.	6.07
AF	41.016893	28.960131	0.33	2.99	0.54	0.07	1.62	37.89	2.433	35.21	n.d.	32.30	16.09	11.93	15.27	73.58	27.94	6.93
AM	41.017017	28.960425	1.12	0.88	0.55	0.08	3.29	48.98	0.258	46.41	45.98	35.62	17.11	13.15	68.01	11.99	8.80	5.40
BB	41.011272	28.965328	2.87	0.34	0.64	0.25	0.32	10.68	0.016	37.25	31.37	n.d.	16.20	20.94	74.00	10.57	13.37	n.d.
BF	41.010680	28.965334	3.54	0.28	0.65	0.31	0.26	7.91	0.001	18.72	32.17	n.d.	15.92	n.d.	68.89	6.80	14.56	n.d.
BM	41.010705	28.964801	0.50	1.99	0.66	0.16	0.59	17.00	0.018	35.23	n.d.	31.26	16.27	11.73	73.44	12.02	16.15	7.31
MB	41.016926	28.949422	0.31	3.20	0.58	0.10	3.43	43.94	0.014	32.86	n.d.	33.39	38.01	11.56	67.54	41.18	n.d.	5.09
MF	41.016950	28.950112	1.96	0.50	0.47	0.16	5.93	45.72	0.266	n.d.	37.44	29.15	n.d.	11.83	80.83	8.56	13.73	6.50
MM	41.017222	28.949822	0.56	1.77	0.52	0.08	2.39	31.05	0.050	38.36	n.d.	32.96	34.68	11.85	69.31	8.56	28.16	7.11
NB	41.010583	28.970841	2.77	0.35	0.59	0.12	0.72	28.89	0.003	12.22	35.46	n.d.	n.d.	n.d.	99.91	8.95	16.06	n.d.
NF	41.010500	28.971104	0.74	1.34	0.54	0.05	4.47	81.42	0.075	36.29	n.d.	33.45	25.97	11.51	82.36	8.57	18.71	6.14
NM	41.010862	28.971184	0.82	1.20	0.47	0.14	0.97	20.84	0.054	39.14	n.d.	32.21	n.d.	12.22	65.72	18.14	12.77	4.68
RB	41.009071	28.958459	1.63	0.61	0.58	0.16	1.68	21.25	0.131	36.37	36.53	32.69	15.50	12.48	63.85	11.61	13.22	7.62
RF	41.009432	28.959325	2.59	0.38	0.60	0.18	1.38	20.29	0.012	9.29	35.19	28.14	14.99	11.28	93.29	9.22	15.10	n.d.
RM	41.009420	28.958463	1.43	0.69	0.63	0.12	1.14	20.23	0.021	41.08	45.55	26.47	15.76	12.00	70.90	7.70	13.33	n.d.
SB	41.016033	28.962626	0.46	2.13	0.46	0.10	7.10	82.34	0.849	26.02	n.d.	34.80	15.69	11.86	83.28	6.97	12.01	5.66
SF	41.015078	28.963559	2.55	0.39	0.66	0.17	0.54	16.14	0.028	n.d.	37.69	32.56	15.98	12.31	75.70	7.26	11.54	n.d.
SM	41.015700	28.963024	2.71	0.36	0.65	0.13	0.93	26.77	0.091	30.07	35.88	n.d.	13.61	n.d.	97.30	6.79	12.91	n.d.

^aLast letters of the codes for locations: B, F, and M: back, front and middle, respectively. Second letter codes for locations: A: Atıf Efendi Library, B: Beyazıt Library, M: Millet Library, N: Nur-u Osmaniye Library, R: Ragıp Paşa Library, S: Süleymaniye Library. ^bWavenumbers in cm⁻¹. ^cPWI: Potential Wettability Index. ^dn.d: could not be determined.

1 2.4. DRIFTS measurements

2 In DRIFTS, IR radiation penetrates the sample to a depth, which is dependent on the
3 reflective and absorptive characteristics of the sample. This partially absorbed light is then
4 diffusely re-emitted from the sample and collected on a mirror that focuses energy coming from
5 the sample onto the detector. The resulting spectrum is comparable to that produced in
6 transmission mode, but is more dependent on spectral properties of the sample interface. IR
7 radiation reflected from the surface of the soil samples was measured by DRIFTS module on a
8 FT-IR spectrometer ALPHA (Bruker Optics, Germany) in the 4000–400 cm^{-1} region (Mid IR
9 range: MIR). All measurements were performed at ambient temperature in the laboratory. The
10 spectra were acquired by 128 scans performed with the spectral resolution of 2 cm^{-1} . Each soil
11 sample was first finely grounded in an agate mortar before spectral measurement. 2 g of each
12 soil samples were used. All raw soil samples were sieved, then weighed after drying in a furnace
13 at 80°C for 2 hours in order to get rid of humidity. Then, samples were weighed again and the
14 weights were found to be between 0.95 and 1.99 g (Table 1). The samples were packed into a
15 sample cup (9 mm in diameter) to achieve a nearly random orientation. The measurement spot
16 over the cup was 2 mm in diameter. After the background measurement was recorded with the
17 reference gold sample, the soil samples were replaced in the sampling cup and spectra were
18 collected. Prior to every measurement, sample cup was cleaned with ethanol (analytical grade
19 of 99%). FTIR spectrometer has CsI (Cesium Iodide) beam splitter, thermo-electrically cooled
20 DTGS (deuterated triglycine sulfate) detector. Spectral resolution is 2 cm^{-1} and the
21 spectrometer has optical (moving mirror) velocity of 0.632 cm/s. The background spectrum
22 was taken every 60 mins. with atmosphere as background. All spectra were normalized to 1 and
23 Kubelka-Munk conversion were applied to each spectrum.

24

25 2.5. Spectral data interpretation

26 All spectral data were interpreted by both OMNIC 8.3.103 software (Thermo Fisher
27 Scientific Inc.) and Spectragryph optical spectroscopy software (Menges, 2020). Firstly, linear
28 baseline correction over the manually specified baseline points was used in OMNIC software.
29 Smoothing operations over 7 points (correspond to 3.375 cm^{-1} in wavenumbers) were
30 performed. It is allowed from 5 to 21 points in an increasing sequence of odd numbers in the
31 software. Kubelka-Munk conversion was applied to the spectra (Kubelka and Munk, 1931).
32 Secondly, all spectra were imported to Spectragryph software and Full Width at Half Maximum
33 (FWHM) of all selected peaks were calculated through the software's implemented algorithms.
34 Peak finding threshold was 0.1 % of visible spectrum ordinate. Search interval and position
35 tolerance were 4 and 0.01 %, respectively. All spectra were interpreted by means of selected
36 peak intensity ratios, PWI, DI, areas under selected curves and selected FWHM values (Table
37 2). Intensity ratios of C-H peaks observed at 2873 and 2924 cm^{-1} and $3669/3640\text{ cm}^{-1}$ were
38 given in Table 2, together with PWI for comparison and differentiation purposes. C-H peaks
39 and their observed positions were reported in previous studies (Unsalan et al., 2015; Unsalan et
40 al., 2012; Billes et al., 2012; Erdogdu et al., 2012; Unsalan et al., 2014). Selected integrated
41 areas were calculated between the ranges of $2825\text{-}3000\text{ cm}^{-1}$ (for three prominent peaks at 2983 ,
42 2924 and 2874 cm^{-1}), $1563\text{-}1753\text{ cm}^{-1}$ (for central peak at 1650 cm^{-1}) and $1029\text{-}1035\text{ cm}^{-1}$ (for
43 central peak at 1032 cm^{-1}). For this purpose, individual integrated baselines were used which
44 were implemented in Spectragryph software. Furthermore, FWHM data for the corresponding
45 bands at 2874 , 2920 , 2515 , 2357 , 1796 , 1636 , 1160 , 810 and 715 cm^{-1} were also given in Table
46 2.

47

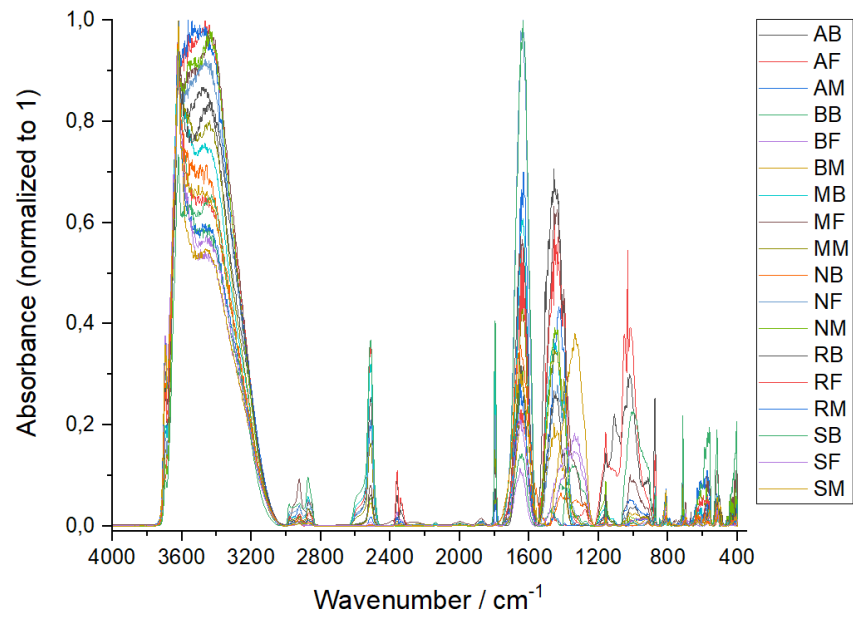
48

49 **3. Results and discussion**

50 *3.1. IR spectroscopy - DRIFTS*

51 DRIFTS is an IR spectroscopic technique used on powder samples with almost no
52 preparation and this technique is an alternative to conventional laboratory methods has been
53 used to determine soil characteristics (soil pH, organic carbon, metal content, water content,
54 clay mineralogy and many others) rapidly and inexpensively. The determination of soil
55 physical, chemical, biological and mineralogical characteristics with conventional laboratory
56 analysis can take great time and be expensive. Furthermore, the accuracy of spectroscopic
57 techniques depends on the calibration and the precision and accuracy of the reference method.
58 Therefore, reliable analytical methods need to be used in calibration of spectroscopic technique
59 used in the analysis.

60 All normalized spectra and observed wavenumbers for the soil samples were given in
61 Table 3. FTIR spectra of 18 soil samples were given in Fig. 3 between 4000 and 400 cm^{-1} .
62 Minerals such as kaolinite, quartz, humic acid, calcite, montmorillonite, goethite, hematite and
63 some possible organic matter (OM) were identified. FTIR spectra of the samples showed that
64 quartz and kaolinite were the most major constituents and other minerals as minor constituents.
65 The results clearly show the connection between natural and traffic related pollution, with well-
66 formed minerals, particularly kaolinite.



67

68 **Fig. 3.** All spectra collected from the soil samples nearby historical libraries in Fatih district,

69 Istanbul, Turkey.

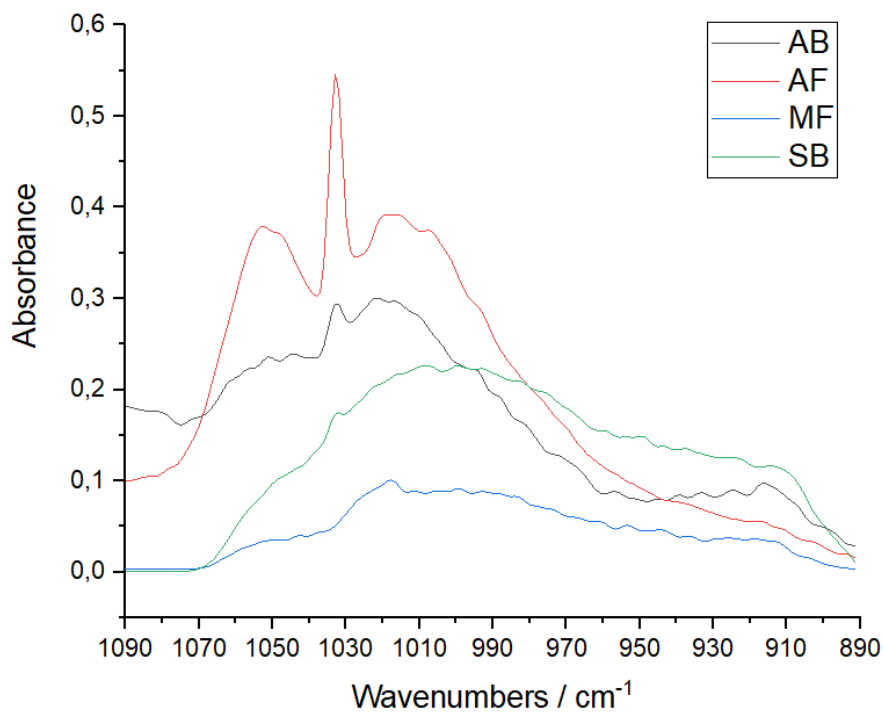
Table 3. FTIR spectral data of the soil samples with their tentative assignments.

A			B			M			N			R			S			Tentative assignments	Minerals
M	F	B	M	F	B	M	F	B	M	F	B	M	F	B	M	F	B		
3695	3696	3697	3698	3696	3696	3695	3696	3695	n.d.	3695	3696	3697	3696	3697	3697	3696	3697	O-H stretching vibration of kaolinite (Al ₂ Si ₂ O ₅ (OH) ₄)	Kaolinite ^{a,b}
3618	3616	3620	3621	3620	3620	3621	3621	3621	3620	3620	3621	3620	3621	3620	3621	3621	3621	O-H stretching in clays or aluminosilicates	Kaolinite ^{a,b}
3465	3467	3475	3465	3466	3465	3465	3462	3468	3456	3466	3464	3467	3468	3460	3462	3460	3451	H-O-H stretching of water molecules in montmorillonite	Montmorillonite ^c
2924	2924	2920	2926	2923	2923	2922	2924	2923	2922	2923	2922	2925	2920	2924	2921	2924	2925	Overtone of carbonate fundamental at 1473 cm ⁻¹	Carbonate ^b
2873	2872	2873	2873	2875	2872	2873	2874	n.d.	2874	2874	2876	2873	2874	2873	2852	2853	2849	Asymmetric CH stretching	O.M.* (n.d.)**
n.d.	2512	n.d.	2512	2510	2515	2513	2514	2513	2512	2512	2515	2511	2510	2512	2515	2514	2513	CaCO ₃ stretching	Calcite ^b
n.d.	n.d.	n.d.	2361	2360	2357	n.d.	n.d.	n.d.	2384	2384	2385	2361	2359	2360	2364	2360	2362	Overtone of Si-O stretching at 1159 cm ⁻¹	Quartz ^b
n.d.	n.d.	n.d.	2342	2342	2341	2348	2349	2348	2348	2348	2348	2342	2342	2342	2342	2342	2343	Carbohydrate overtone	Calcite ⁱ
1887	1887	1890	1890	1887	1890	1890	1891	1891	1891	1891	1891	1889	1891	1890	1890	1890	1890	Carbohydrate overtone	n.d.
1866	1866	1869	1871	1870	1870	1878	1873	1872	1872	1872	1872	1869	1871	1870	1870	1870	1870	Si-O stretching	Quartz ^b
1796	1796	1794	1795	1795	1793	1796	1796	1796	1795	1796	n.d.	1794	1795	1795	1793	1794	1797	Si-O stretching	Quartz ^b
1637	1633	1637	1638	1636	1633	1637	1640	1636	1638	1636	1651	1653	1654	1654	1654	1653	1636	Protein amid peak (C=O) or calcite/illite (Islam, 2019)	Protein ^d /calcite/illite
1485	1454	1458	1457	1456	1457	1457	1457	1455	1459	1457	n.d.	1457	1457	1458	1457	1457	1473	Carbonate fundamental vibration	Carbonate ^b
1428	1434	1430	n.d.	n.d.	n.d.	n.d.	n.d.	n.d.	1437	1436	1418	1420	1421	n.d.	1419	1418	n.d.	CaCO ₃ asymmetric bending or amide C-N	Calcite or amide: n.d.
n.d.	n.d.	n.d.	1401	1398	1404	1401	1401	1400	1395	1400	n.d.	1396	1398	1400	1397	1394	1387	OH deformation and C-O stretching of phenolic OH ⁱ	n.d.
n.d.	n.d.	n.d.	1160	1160	1159	1159	1159	1162	1159	1159	1160	1159	1159	1159	1159	1159	1159	Si-O stretching	Quartz ^b
1102	1107	1108	1111	1112	1110	1110	1112	n.d.	1112	1109	1109	1110	1114	1115	1111	1111	1111	Si-O stretching	Quartz ^b
n.d.	n.d.	n.d.	1057	1056	1057	1056	1056	1060	1058	1056	1056	1057	1056	1050	1051	1053	n.d.	(ν ₃) mode of carbonate	Carbonate ^b
1033	1033	1032	1032	1033	1033	1033	n.d.	1033	1033	1033	1033	1033	1032	1033	1033	1032	1032	Na-montmorillonite	Montmorillonite ^c
n.d.	n.d.	n.d.	1018	1018	1019	1016	1018	1020	1018	1016	1020	1017	1017	1016	1020	1018	1008	O-Si-O stretching	Kaolinite ^b
911	911	916	912	916	915	914	918	911	925	912	915	928	934	923	921	921	924	Na-montmorillonite	Kaolinite ^{a,b}
874	874	876	876	880	875	875	876	874	875	874	872	875	873	875	878	873	872	Na-montmorillonite	Montmorillonite ^c
848	848	848	848	848	844	848	848	848	849	848	848	847	836	848	n.d.	848	848	Fe-O stretching in goethite (FeOOH)	Montmorillonite ^c
812	809	811	811	812	810	814	813	n.d.	812	817	814	812	813	811	813	813	813	NO ₃ ⁻²	Nitrate ^j
791	791	792	791	790	789	794	792	797	798	796	799	792	794	792	792	791	791	Fe-O stretching in goethite (FeOOH)	Goethite ^{e,f}
715	714	715	714	718	714	715	714	715	714	715	715	715	714	714	711	712	715	Calcite vibrations	Calcite ^{b,g}
633	632	632	630	635	629	n.d.	n.d.	n.d.	632	632	639	632	632	629	633	629	632	Fe-O stretching in goethite	Goethite ^{e,h}
n.d.	n.d.	n.d.	512	514	512	516	514	n.d.	517	517	515	515	511	516	516	517	519	Fe-O stretching in hematite (Fe ₂ O ₃)	Hematite ^c
498	n.d.	495	500	497	504	n.d.	n.d.	n.d.	497	499	499	498	496	495	490	492	495	S-O bending vibration for sulfite	Sulfite ^j
465	465	462	469	469	466	468	468	462	466	463	456	446	440	440	444	443	442	Fe-O vibrations	Hematite ^{e,h}
404	405	406	409	406	408	402	405	402	406	410	409	405	410	409	405	403	406	Fe-OH asymmetric stretching	Goethite ^{e,h}

First letter of the codes for locations: B, F, and M: back, front and middle, respectively. Second letter codes for locations: A: Atf Efendi Library, B: Beyazıt Library, M: Millet Library, N: Nur-u Osmaniye Library, R: Ragıp Paşa Library, S: Süleymaniye Library. *O.M.: Organic matter, **n.d.: not determined, ^{a,b} (Cannane et al., 2013; Nguyen et al., 1991), ^c (Kaluderović et al., 2018), ^d (Calderon et al., 2011), ^e (Parikh et al., 2014), ^f (Blanch et al., 2008), ^g (Messerschmidt, 1985), ^h (Schwertmann and Taylor, 1989), ⁱ Islam et al., 2019, ^j Verma and Deb, 2007b; Wang et al., 2017.

70 3.1.1. Kaolinite ($Al_2Si_2O_5(OH)_4$)

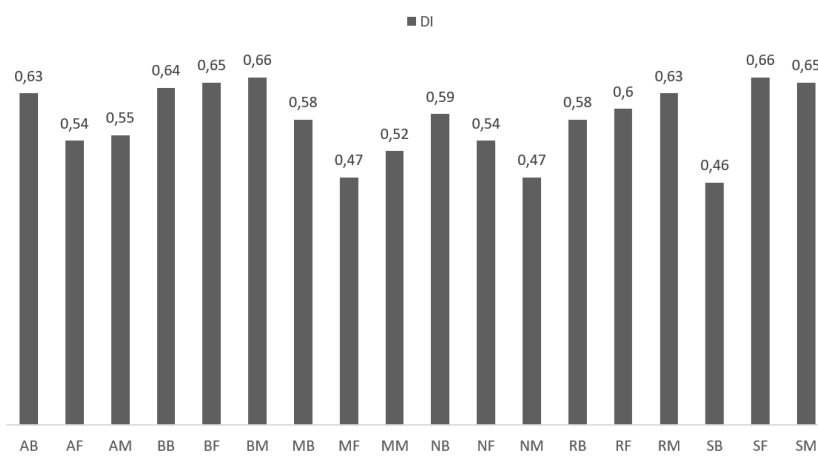
71 Kaolinite was detected by its representative bands observed at 3697, 3621, 1008 and
72 924 cm^{-1} . Our findings for kaolinite were consistent with previous results by Nguyen et al.
73 (1991) who reported these bands at 3698, 3622, 1020 and 920 cm^{-1} (Nguyen et al., 1991). One
74 of the most recent studies performed on geochemical, mineralogical and morphological
75 characterisation of road dust revealed that kaolinite was observed among the other minerals like
76 albite, muscovite and graphite (Candeias et al., 2020). On the other hand, not only the natural
77 but also the anthropogenic contributions must also be considered for these sort of investigations.
78 It is known that lattice vibrations near 1020 and 920 cm^{-1} generally shift or broaden depending
79 on the crystal structure, variations in the hydrogen bonding and lattice ordering (Russell, 1987;
80 van der Marel and Beutelspacher, 1976). We also observed these broadening and shift effects
81 for these peaks only for AB, AF, MF and SB samples (Fig. 4) near the mentioned peaks.



82

83 **Fig. 4.** Broadening and shifting effect for kaolinite for AB, AF, MF and SB soil samples.

84 After baseline correction, DI, a quantitative relation between the relative intensities of
 85 the bands at 3669 and 3650 cm^{-1} was found that they were previously defined for kaolinites
 86 (Delineau et al., 1994). Based on our results obtained for DI, we confirm that kaolinite is very
 87 sensitive to environmental accumulations as previously reported by several works (Delineau et
 88 al., 1994; Gonzalez-Grijalva et al., 2019; Leue et al., 2013). We found and confirm that kaolinite
 89 data based on DI is in generally in accordance with the locations where the samples collected
 90 (Fig. 5 and Table 2) that are close to heavy traffic.



91 **Fig. 5.** DI for all samples with respect to their location codes.

92
 93
 94 **3.1.1.1 Atıf Efendi Library (AB, AF, AM)**

95
 96 Results tabulated in Table 2 suggest that AB has higher DI (0.63) compared to AF (0.54)
 97 and AM (0.55) (Fig. 5) which is an indication of more adsorbed pollutant contamination on the
 98 soil sample from AB (Fig 2). In addition, AB is the spot where the library is located and this
 99 location might be evaluated under pollution risk due to its higher DI, but of course there might
 100 be several possible sources of contamination that cause this contribution. One another reason
 101 for this high DI data for AB, it is close to a main road (Atatürk Boulevard) which connects
 102 seaside to Taksim square and due to the traffic in this main road, it is highly possible that AB
 103 experienced this pollution. Moreover, there is a Roman Empire aqueduct (Valence

104 Aqueduct:VA) which intersects this main road and we think that our conclusion is also
105 meaningful based on our previous Raman spectroscopic and structural work on the columns of
106 VA (Unsalan and Kuzucuoglu, 2016) which we observed pollution on its columns. However,
107 more careful investigations are required at this point. Besides, next to AB, there is a car park
108 which could contribute to change DI data and pollution (Fig. S1). In addition, nearby AF, there
109 are three open car parks and one larger parking area near AM. Even this latter parking place
110 contain many cars, interestingly AM has the moderate DI (0.55). This might be explained by
111 unidentified different factors that might have affected this spot.

112

113 *3.1.1.2 Beyazit Library (BB, BF, BM)*

114

115 Beyazit Library, located in Beyazit square, is next to BF (DI: 0.65) and there is a parking
116 place in front of the library building. Almost every day, many visitors including researchers or
117 public enter this building. Even it is not publicly allowed to park just in front of this building,
118 authorities of library frequently use this parking space. Consequently, some certain amount of
119 pollution by the cars parked in this area has to be taken into account. Furthermore, BB (DI:0.64)
120 is next to the street which is exposing a traffic everyday even if it has the least DI data. BM has
121 the highest DI value of 0.66 and this is because there is a public parking place just behind this
122 spot, hence it is clear that the soil sample from this point was highly affected by pollution
123 produced by cars, mainly exhaust products. It is interesting to note that, although there is a big
124 parking place really close to BF, we obtained moderate DI value of 0.65, unexpectedly. This
125 might be explained by some other unknown and forecasted factors that could have affected our
126 results.

127

128

129 *3.1.1.3 Millet Library (MB, MF, BM)*

130

131 Millet Library is at a location where it crosses a connection street (Fevzi Paşa street:
132 hereafter, FS) and also close to Vatan road (VR) in southwest of FS and VR is one of the other
133 main connection roads like Atatürk Boulevard (ATB). Our results revealed that MB has the
134 highest DI (0.58) which states that the library itself suffered from pollution and might be
135 considered at under risk. MF and MM differ from MB with the DI data of 0.47 and 0.52,
136 respectively. It seems that a parking place next to the block, where the library located,
137 contributes more than the FS itself. This may be explained with the regular and direct exposure
138 of the library to the exhaust gases frequently by parking cars. On the other hand, even though
139 MF and MM are closer to the street than MB, one less possible factor that may have increased
140 the pollution of this location is that MB is close to ATB from the southwestern facet of the
141 building, which is wider than FS, thus carries heavier traffic compared to FS. Of course, that is
142 not an easy task to precisely identify the reason of pollution.

143 *3.1.1.4 Nur-u Osmaniye Library (NB, NF, NM)*

144 Nur-u Osmaniye library, located in the Nur-u Osmaniye mosque complex, is close to
145 Çemberlitaş open parking place which is immediately south of the mosque. Together with the
146 relatively light traffic in Vezirhan street (VS), this parking place would have contributed to
147 pollution of this library's backyard (NB) to a certain degree of DI of 0.59. It is also obvious that
148 total recoverable hydrocarbon (TRH) contribute the maximum amount of pollution at NM (red
149 star in Fig. 2 (See section 3.1.10).

150

151

152

153 *3.1.1.5 Ragıp Paşa Library (RB, RF, RM)*

154

155 Samples collected from RM and RF were very close to a wide street (Ordu Street: OS)
156 and exposed to heavy traffic and our results were satisfactory for DI data especially for RM and
157 RF, 0.63 and 0.60, respectively. RF, RM and RB regions revealed an increasing order for B, F,
158 and M respectively. Due to the exposure of heavy traffic, soil samples from these spots might
159 have been depleted in various contaminants and spectral signals for kaolinite was consequently
160 affected. Since there is not much parking place in the proximity of Ragıp Paşa Library, the
161 main reason for the pollution for this area seems to be OS and its traffic load itself.

162

163 *3.1.1.6 Süleymaniye Library (SB, SF, SM)*

164

165 Süleymaniye library is in Süleymaniye Mosque complex and it was found that DI data
166 was in increasing order for SB (DI:0.46), SM (DI:0.65) and SF (DI:0.66), respectively where
167 the closest spot to traffic pollution is SF. Location of SF is indeed next to the street which is
168 already open to a traffic (“Prof. Dr. Sıddık Sami Onar street” which is seen Fig. 2).
169 Consequently, our findings based on DI data derived from kaolinite, extend our knowledge of
170 pollution can be attributed to kaolinite’s adsorption capability, thus we can confirm that DI
171 related to kaolinite would be used as a key parameter basis for determination of air pollution
172 and risk assesment of places that are particularly important for cultural heritage.

173 *3.1.2 Quartz (SiO₂)*

174 Fundamental O-Si-O stretching and bending wavenumbers at 1080, 800-700 and 700
175 cm⁻¹ were reported to be the most dominant bands in FTIR spectra of quartz-rich soils (Nguyen
176 et al., 1991; Soda, 1961). Unlike what was previously found for quartz by Nguyen et al. (1991)
177 and Soda (1961), we did not observe strong and intense bands for quartz which led us to

178 conclude quartz-poor soils in our case. For example, we did not observe characteristic peak of
 179 quartz at 1080 cm^{-1} in any of our spectra. However, a doublet at around 800 cm^{-1} is a descriptive
 180 for quartz (Nguyen et al., 1991) and this doublet can be used as a quick diagnostic peak for
 181 quartz. Although we concluded that our samples were quartz-poor soils, we observed this quartz
 182 doublet with weak intensities (maximum around 0.073) approximately at 792 and 813 cm^{-1}
 183 (Fig. 6) which indicates that we have at least some amount of quartz in all our samples.
 184 According to Table 4, maximum intensities of the peaks for 813 cm^{-1} is in consistency with the
 185 locations of the collection spots where traffic is close. For example, RM (0.073) and RF (0.065)
 186 are closer to the traffic than RB (0.047) which means that quartz is also sensitive to pollution
 187 (Fig. 6). MF (0.071), MM (0.018) and MB (0.010) are in decreasing order and this is inversely
 188 proportional to the DI data (0.47, 0.52 and 0.58).

Table 4. Intensity maxima of quartz peaks at 813 and 792 cm^{-1} (in decreasing order).

Site	Max. intensity at 813 cm^{-1}	Site	Max. intensity at 792 cm^{-1}
RM	0.073854	RM	0.016639
MF	0.071535	MF	0.016282
SM	0.070358	RB	0.015145
RF	0.065621	NM	0.013047
SB	0.051133	MM	0.012893
RB	0.047342	MB	0.012030
NM	0.042894	AB	0.011079
SF	0.039930	BM	0.010015
BF	0.026029	SM	0.009504
NB	0.022404	RF	0.009158
BM	0.021323	AF	0.008321
BB	0.019770	SF	0.007545
AM	0.019086	BF	0.006870
MM	0.018702	NB	0.006810
AF	0.012702	BB	0.006791
NF	0.011916	SB	0.006684
MB	0.010933	AM	0.005471
AB	0.009877	NF	0.005425

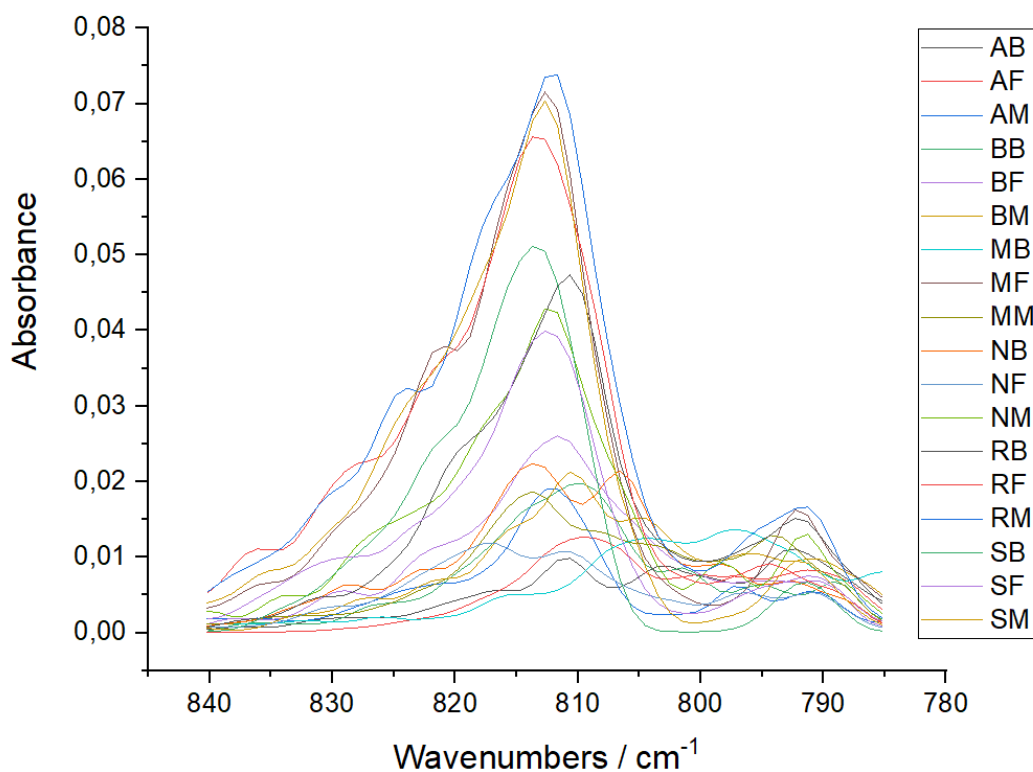


Fig. 6. Diagnostic quartz doublet (813/792 cm^{-1}) at around 800 cm^{-1} peak.

189

190

191

192 3.1.3. Humic acid (HA) content

193 As hypothesized by (Calderon et al., 2011), the peak observed at 1340 cm^{-1} is attributed

194 to humic acid which indicates a stronger absorbance of the soil carbon (C) than the microbial

195 material due to phenolic or COO stretching vibrations in more oxidized soil C (Calderon et al.,

196 2011). Authors also highlighted that 1640 cm^{-1} peak is related to protein content, mainly caused

197 by casein. We observed these possible protein peaks approximately at 1640 cm^{-1} in all spectra

198 as second intense peak group after the most intense peak groups in the region of 3600-3000

199 cm^{-1} (Fig. 3). Based on their results, microbial proteins in soils strongly affect this absorbance

200 value. We observed peaks related to 1340 cm^{-1} peak, only for SM (1336 cm^{-1}), SF (1341 cm^{-1}),

201 BB (1338 cm^{-1}) and BF (1338 cm^{-1}) soil samples. At this point, we can qualitatively speculate

202 that the spots where these four samples could have HA content. Furthermore, it must also be

203 emphasized that it is not an easy task to qualify the amount and the origin of humic acid.

204 3.1.4. Calcite (CaCO_3)

205 It is known that pure calcite shows characteristic peaks at 2988, 2880, 2517, 1800, 1470,
206 875 and 720 cm^{-1} (Messerschmidt, 1985). Nguyen et al. (1991) showed that some bands at 2592
207 and 2517 cm^{-1} can be used to diagnose calcite (Nguyen et al., 1991). For this reason, authors
208 used the bands around 2500 cm^{-1} to identify calcite and we used these descriptive bands to
209 detect calcite in our spectra (Fig. 3) around 2500 cm^{-1} . We observed calcite at 2925, 2513, 1870,
210 1797 and 715 cm^{-1} in our spectra and, based on previous works (Messerschmidt, 1985; Nguyen
211 et al., 1991), our results confirm the presence of calcite and further support the role of these
212 definitive peaks for calcite.

213 Data obtained from the collection locations showed that calcite vibrations (Table 3)
214 were not strongly correlated with the traffic-bearing locations and pollution. This was also
215 confirmed for calcite fundamental vibrations observed at approximately at 1457 cm^{-1} with the
216 only one exception for SB which gave a band at 1473 cm^{-1} that is very high wavenumber
217 compared to other locations. At this point, we can not rule out that any other type of mineral
218 rather than calcite may have influenced the reflectance due to its grain size, or any other reason
219 that we could not determine, and this band was observed at higher value. Furthermore,
220 wavenumbers observed around 715 cm^{-1} do not alter according to the locations and no
221 correlation was observed for this vibration as a result. We should also mention that Total
222 Recoverable Hydrocarbon (TRH) content (Table 6) for the locations revealed that backyards of
223 the sample collection spots exhibited the highest amount of TRH which is in consistency with
224 wavenumbers observed at higher numbers for calcite. We also saw no significant difference in
225 observed vibrational wavenumber at around 715 cm^{-1} for calcite.

226

227

228 *3.1.5. Montmorillonite, goethite and hematite*

229

230 *Montmorillonite*

231 TRH content was compare to observed absorbance peaks of montmorillonite and
232 positive correlation was observed with the higher wavenumbers of montmorillonite and TRH
233 content. All TRH data observed were related to higher wavenumber of corresponding
234 montmorillonite wavenumbers at around 3460 cm^{-1} . However, we could not observe any
235 significant and sensitive band for Na-montmorillonite around 1032, 873 and 848 cm^{-1} (Table
236 3) and we can conclude that Na-montmorillonite can not be a sensitivie tool to monitor traffic-
237 born air pollution. To the best of our knowledge, this is the first connection between TRH and
238 montmorillonite data we presented here.

239

240 *Goethite*

241 It is previously reported that differences in the coordination of Fe with O cause certain
242 Fe-O and Fe-OH absorbances at 3400–3000 cm^{-1} , 900–700 cm^{-1} , and $<700 \text{ cm}^{-1}$. O-H stretching
243 absorbance bands and bending reflect the degree of cation substitution. For instance, increasing
244 Al substitution in goethite causes a wavenumber increase and band broadening for O-H
245 stretching at 3153 cm^{-1} and in-plane and out-of-plane O-H deformation at 839 and 894 cm^{-1} .
246 Band broadening can also reflect decreasing crystallinity (Margenot et. al, 2017). We observed
247 goethite peak at around 799, 639 and 405 cm^{-1} (Table 3).

248 When we compared the IR spectra and SO_2 data for the peak around 405 cm^{-1} in IR
249 spectra, we interestingly found that all locations with higher SO_2 value are directly proportional
250 to the higher wavenumbers for goethite. For example, goethite was observed at 406 cm^{-1} for
251 AB and this is consistent with the highest amount of SO_2 (1.58) (Table 5). However, 799 and
252 639 cm^{-1} peaks were compared and no significant relation between goethite and SO_2 have been

253 found. Consequently, we concluded that there might be a relationship between SO₂ data with
254 the goethite in terms of traffic-driven air pollution which needs further investigation and might
255 require an attention in another study.

256

257 *Hematite*

258 Hematite exhibits a single band at around 3697 cm⁻¹. This reflects that our samples
259 contain 2:1 layers of certain silicates. The bands at around 2925-2920 cm⁻¹ represent aliphatic
260 C-H vibration of aliphatic methyl and methylene groups. Observed broad band at 2600 cm⁻¹
261 was attributed to the formation of intermolecular hydrogen bonding between OH groups in
262 oxygenated compounds (Forrester et al., 2013; Montecchio et al., 2006). The band located
263 above 1600 cm⁻¹ is caused by the Al-OH and Si-OH stretching of aluminosilicates near 3625
264 cm⁻¹. Natural sediments or soils also contain interlayer hydrogen-bonded water molecules that
265 are responsible for a broad absorption around 3650 and 3000 cm⁻¹ mainly centered at 3400 cm⁻¹
266 (Koretsky et al., 1997; Bishop et al., 1996; Pieteres et al., 1993; Bellamy, 1975). We also
267 investigated whether there is a relationship between hematite bands and TRH and/or SO₂/TRH
268 content and no significant change was observed specifically for hematite. Thus, we can
269 generally conclude that there is no relation between these parameters.

270

271 *3.1.8 Sulphur dioxide (SO₂) as a pollutant*

272 We were able to detect sulphur dioxide in the form of SO₃²⁻ in IR spectra. Sulphur
273 dioxide was detected by its representative peaks at 495 and 632 cm⁻¹ (Verma et al., 2007). From
274 the intensity values at these observed wavenumbers for all samples, we could quantitatively
275 determine the amount of sulfite adsorbed on our soil samples. According to our results, SO₂
276 concentrations in our soil samples varied from 0.05 to 1.84 µg (Table 5). In addition, our
277 findings are in good agreement with earlier study performed by (Verma et al., 2007). In that

278 study, they found this range between 0.05–5 μg . When the areas under each curve were
279 considered, no significant data was extracted regarding SO_2 concentrations, so they were not
280 included in our evaluation. It must be emphasized that we did not take the area data under 495
281 cm^{-1} peak into account because this data did not give significant results unlike the findings of
282 previous report (Verma et al., 2007). There is acceptable agreement with the SO_2 data with our
283 DI extracted from kaolinite based spectral results. For example, AB possess the greatest DI
284 among the AF and AM and SO_2 concentration for AB (1.58 μg) is he highest value among AF
285 and AM, so this is in consistent with our DI findings. Besides, SO_2 concentrations were seen in
286 good agreement with the absorbance intensities observed for the peak at 495 cm^{-1} . This clearly
287 indicates that we can use this band as a diagnostic tool to show the relationship between SO_2
288 concentration and maximum intensity at 495 cm^{-1} observed in IR spectra of urban topsoils
289 investigated in this study.

290

291

292

293

294

295

296

297

298

299

300

Table 5. SO₂ concentration of the urban topsoils in this study.

Sample spot	Maximum intensity at 495 cm ⁻¹	SO ₂ concentration (µg)	Comment
AB	0.032167	1.58	Open parking lot OPL)
AF	0.000702	-0.09	Near the street (NTS)
AM	0.003613	0.06	Far from street (FFS)
BB	0.009578	0.38	NTS
BF	0.006493	0.22	Car parking area (CPA)
BM	0.037155	1.84	OPL
MB	0.010328	0.42	CPA
MF	0.003563	0.06	NTS
MM	0.012370	0.53	OPL
NB	0.011462	0.48	OPL
NF	0.001515	-0.05	NTS
NM	0.015673	0.70	NTS
RB	0.004121	0.09	OPL
RF	0.003470	0.05	NTS
RM	0.001499	-0.05	NTS
SB	0.000249	-0.12	FFS
SF	0.001591	-0.04 traffic	NTS
SM	0.001596	-0.04 traffic	CPA

SO₂ concentration data is based on the calibration curve from Verma et al., (2007) by a calibration data yielded a linear equation: $y = ax + b$. Here, y is the absorbance at 495 cm⁻¹ and x is concentration of SO₂. a and b are 0.0024344725 and 0.018833027. T: Close to traffic, C: Car parking area. Car parking area data are from Istanbul Metropolitan Municipality's official website by spotting the open air car parking areas www.sehirharitasi.ibb.gov.tr.

301

302 3.1.9. Sulfate (SO₄²⁻), sulfite (SO₃²⁻) and nitrate (NO₃⁻) identification

303 Regarding nitrate, we did not observe any peaks associated with any nitrate (NO₃⁻)
304 components which were previously reported at 1385, 1050, 832-837, 712-719 cm⁻¹ (Verma and
305 Deb, 2007b). Sulphate (SO₄²⁻) bands were also found to be detected at 1117, 983, 617 cm⁻¹
306 (Verma and Deb, 2007a) and 552 cm⁻¹ (Wang et al., 2017). SO₃²⁻ was also identified by its
307 characteristic peak at 698 cm⁻¹ (Verma and Deb, 2007b). However, even though it was not
308 reported by work of Verma and Deb (2007b), in an investigation that evaluated the risk
309 assesment on heavy metals in soils, it was shown that the peak observed at 815 cm⁻¹ can be
310 used as a diagnostic tool for NO₃⁻ (Wang et al., 2017). We observed this peak in our samples

311 around 810 cm⁻¹ (Table 3) and were able to observe the existence of NO₃⁻ as a possible
312 anthropogenic factor caused by exhaust gases.

313

314 *3.1.10. Prediction of Total Recoverable Hydrocarbon (TRH)*

315

316 It has been proposed that spectra obtained by DRIFTS can be used for development of
317 prediction of TRH concentrations in contaminated soils collected from sites in southern
318 Australia known to be contaminated with TRH. Authors have shown that detailed analysis of
319 contamination of soils has become available by DRIFTS (Forrester et al., 2013). A quite large
320 review has been published on the use of various spectroscopic techniques such as UV-Visible,
321 portable X-Ray Fluorescence (pXRF) and Visible and Near IR (Vis-NIR) on determination of
322 soil contamination (Horta et al., 2015). According to a recent research, detailed IR analyses on
323 soil contaminants revealed that selected IR peaks and relevant areas under these corresponding
324 certain peaks are helpful in identifying the amount of Total Recoverable Hydrocarbon (TRH)
325 concentration in soils together with the aid of multiple regression model. Based on the results
326 and correlation equations derived by Ng et al. (2017), we were able to determine approximate
327 TRH content in our soil samples. We found that our TRH contents (Table 6) are in the range of
328 reported by (Ng et al., 2017). Even though further data collection is required to obtain more
329 precise results and construct a more robust model, we can still say that our findings are in
330 acceptable limits with what was reported by Ng et al. (2017).

331 In our research, TRH content was predicted to be between 1013-8421 ppm and 1501-
332 17349 ppm for positive TRH values. Despite the lack of more data collection and regression
333 analysis, we still believe our findings compare well with the TRH results of Ng et al. (2017).
334 Besides, the locations of the nearby car parking places support the results (Figs. S1-S6 and Fig.
335 2). Furthermore, Ng et al. (2017) successfully showed that petroleum hydrocarbon peak

336 characteristics in the C-H region of 2990-2810 cm^{-1} give detailed information on TRH source.
337 They have suggested that the higher the concentration of hydrocarbon contamination was, the
338 higher the absorption peaks. In our work, the spots that are closer to either car parking places
339 or heavy traffic exhibit more TRH content and our findings are in acceptable accordance with
340 the ones reported by Ng et al. (2017) (Table 6 and Figs S1-S6). They also showed that clayey
341 soil that contain finer particles scatter more light than sandy soil, thus reducing the absorbance.

342 Table 6 summarizes the TRH content of the historical library sites where the samples
343 were collected. The spots that are either nearby car parking areas or expose to heavy traffic
344 were also commented in Table 6. According to Table 6, AB, BB, MB, NM, RB and SF suffer
345 most from pollution based on their high amount of TRH. These highly polluted spots were also
346 indicated with “red star mark” in Figs S1-6 and TRH data is in consistent with their location
347 whether they are in the proximity of traffic or car parking areas.

348 Our study also showed that TRH related peaks have high amount of absorbance and this
349 is another confirmation that we can use sandy (mainly kaolinite based) spectral features as a
350 further air pollution diagnostic tool. Another supporting study was performed by Forrester et
351 al. (2010) and the researchers demonstrated that porous clay minerals resulted in a weaker
352 signal compared to non-porous sand. Clay minerals reflect more of the sorbed total petroleum
353 hydrocarbon (TPH) spectra signal because it shielded the TPH within the soil structure
354 (Forrester et al., 2010). This type of quantification of TPH or TRH can be improved and further
355 developed when more observations are done in the near future.

356

Table 6. Prediction of approximate content TRH (ppm) using spectra for the curves based on the data from Ng et al., (2017).

Sample site	A	B	C	D	TRH content (ppm) ^a	TRH content (ppm) ^b	Comment
AB	-0.93604	0.02035	0.02153	1.90460	5783	13470	T,C (Atatürk Boulevard)
AF	-0.14768	0.32725	0.26552	1.62260	1423	5635	C (Near street)
AM	0.73871	0.19457	0.19533	3.30490	<i>-2120</i>	<i>-1303</i>	T
BB	-0.44012	0.35770	0.22152	0.32600	1978	7177	T
BF	-0.43255	0.23737	0.12311	0.26430	1799	6984	C
BM	-0.33290	0.15645	0.12696	0.58940	1433	6266	C
MB	-1.16080	0.12490	0.06085	3.41870	8421	17349	C
MF	0.09067	0.44268	0.30483	5.93710	3936	7987	T
MM	-0.64850	0.27161	0.21615	2.40830	4817	11324	T
NB	0.17568	0.14922	0.06415	0.72652	<i>-1218</i>	1501	C
NF	1.37610	0.09251	0.04583	4.44680	<i>-4677</i>	<i>-6290</i>	T
NM	-1.22620	0.11651	0.06750	0.98054	6670	15385	T
RB	-0.88708	0.25147	0.16007	1.67940	5511	12898	C
RF	0.14548	0.19844	0.15266	1.37820	<i>-485</i>	2469	T
RM	-0.27061	0.29297	0.25112	1.14570	1657	6300	T
SB	2.17910	0.24737	0.29257	7.04970	<i>-6816</i>	<i>-11378</i>	C
SF	-0.26043	0.16115	0.10218	0.54095	1013	5534	T
SM	0.19164	0.13853	0.11056	0.92871	<i>-1172</i>	1511	C

^aPortable IR,^bLaboratory IR (our data is adopted according to Ng et al., (2017)). *Italic* numbers for TRH were not included in our evaluation, since they have negative value. TRH data was extracted as a rough approximation from the equations reported by Ng et al., (2017) which are as follows: Equation (1) for data recorded by portable IR spectrometer is: $-1015 - 5500A + 1176B - 581C + 860D$, and Equation (2) for data recorded by laboratory IR spectrometer is: $2328 - 9739A + 1108B - 812C + 1061D$. These locations are either very close to car parking spaces next to them or close to main road/(s). Here, A is the area between the region 1630-1580 cm^{-1} , B is the area between the region 1930-1845 cm^{-1} , C is the area between the region 2060-1930 cm^{-1} , D is the area between the region 3000-2825 cm^{-1} . T: Close to traffic, C: Car parking area. Car parking area data are from Istanbul Metropolitan Municipality's official website by spotting the open air car parking areas www.sehirharitasi.ibb.gov.tr.

358 *3.2. Correlation between the selected parameters from IR spectra*

359 The statistically significant correlation coefficients (r) ($0 < r < 1$) were obtained from
360 correlation analysis implemented in Microsoft Excel and this correlation analysis was presented
361 in Table 7. This relationship gives an approximate idea on selecting the parameter/(s) that will
362 be used for evaluation. Here, only the strong positive correlations ($r \geq 0.45$) were taken into
363 account. The most four prominent correlated parameters were commented here in order to show
364 the closest correlation between the selected parameters. The strongest correlation ($r = 0.89$)
365 among these four parameters was found only between 1/CH intensity ratio (REV) and FWHM
366 value of 2920 cm^{-1} peak. Second correlated parameters were the “area under the C-H” peaks
367 (CHA) and the area under the 1650 cm^{-1} peak ($r = 0.88$). Third related parameters were the area
368 under 1032 cm^{-1} peak and FWHM of the peak observed at 1160 cm^{-1} ($r = 0.80$). Last correlated
369 parameters were REV and FWHM of the 1160 cm^{-1} peak stands for the quartz ($r = 0.72$).
370 According to Table 7, we can highlight that the most useful indication that make our results
371 meaningful can be between REV and FWHM at 2920 cm^{-1} carbonate peak (Table 3). On the
372 other hand, it was observed that PWI is in only moderate correlation ($r = 0.62$) with 1796 cm^{-1}
373 peak observed for quartz (Table 3) which can be concluded as a moderate contribution and can
374 be used for diagnostic tool.

375 Contrary to our expectation, we observed less significant correlation ($r = 0.73$) between
376 TRH and 2874 cm^{-1} band intensity when compared to REV and CHA. This is very likely
377 probable that the amount of the traffic would change in time and cause fluctuations on the
378 spectra of the samples collected and more systematic and controlled experiments are required
379 in order to get more correlated results. These unexpected inconsistencies can also be explained
380 by several key parameters: 1) the number of the samples for this study, 2) collection date of the
381 samples and 3) the season when the samples collected. Firstly, it is particularly important that
382 more samples are required to get more precise data. Our investigation so far have only been on

383 a small scale and our findings can be regarded as a preliminary study. Secondly, the collection
384 time of the samples is another key parameter due to the traffic depends on the working hours
385 and thus, rush hours can strongly affect the results. In rush hours, there is an increasing amount
386 of deposition of numerous pollutants on the samples (fluctuations) and this contributes to
387 spectral features such as intensity, FWHM and band position depending on the composition and
388 the quantity of that pollutant. Since C-H peaks are highly sensitive to these fluctuations, they
389 immediately response to this change by their intensities. Lastly, the seasons have strong effect
390 on humidity, chemical content and wetness for the soil samples. As an example, rain and wind
391 make the soils wet and the mineral are in interaction with the water deposited by rain and
392 eventually the resultant spectra will be complicated to evaluate and comment. On the other
393 hand, we also suggest that it is also possible to use the correlation between TRH, CHA, and
394 REV data together in order to get qualitative and even quantitative data on pollution for urban
395 topsoils in future. Moreover, our previous efforts showed that the spectroscopic techniques (IR
396 and Raman spectroscopy), especially when coupled with structural analysis (Scanning Electron
397 Microscopy), information and documentation techniques together with Geographical
398 Information Systems (GIS), can play an important role especially in determination of pollutants
399 on the facets of cultural assests such as Valence Aqueduct (Unsalan and Kuzucuoglu, 2016),
400 identification of deterioration level of bindings of the historical books (Unsalan et al., 2017)
401 and old manuscripts (15th century) in libraries (Kuzucuoglu et al., 2015). These findings
402 validate the usefulness of DRIFTS particularly for the pollution caused by traffic within the
403 environment of the selected spots.

404

405

406

Table 7. Correlation between the selected parameters from IR spectra.*

	LAT	LONG	INT	REV	DI	TRH	PWI	CHA	1650A	1032A	2874	2920	2515	2357	1796	1636	1160	810	715	
LAT	1																			
LONG	-0.55	1																		
INT	-0.35	0.26	1																	
REV	0.46	-0.31	-0.85	1																
DI	-0.38	0.18	0.55	-0.35	1															
TRH	-0.24	0.16	-0.29	-0.01	0.00	1														
PWI	-0.42	0.15	0.75	-0.55	0.50	-0.18	1													
CHA	0.48	-0.34	-0.47	0.35	-0.74	-0.04	-0.47	1												
1650A	0.39	-0.04	-0.55	0.43	-0.65	0.08	-0.68	0.88	1											
1032A	0.41	-0.07	-0.39	0.55	-0.33	-0.32	-0.35	0.21	0.29	1										
2874	0.29	-0.20	-0.57	0.29	-0.20	0.73	-0.37	0.13	0.13	0.10	1									
2920	0.28	-0.37	-0.86	0.89	-0.28	0.41	-0.76	0.37	0.58	0.46	0.59	1								
2515	0.48	0.18	-0.49	0.41	-0.32	0.23	-0.52	0.33	0.51	0.18	0.33	0.14	1							
2357	0.39	-0.61	-0.51	0.56	-0.35	0.10	-0.41	0.32	0.30	-0.18	0.21	0.34	0.28	1						
1796	-0.14	0.22	0.51	-0.34	0.31	0.24	0.62	-0.32	-0.33	-0.12	0.22	-0.50	0.42	-0.21	1					
1636	-0.25	0.20	0.47	-0.57	0.16	0.07	0.16	0.08	0.06	-0.74	-0.47	-0.29	-0.18	-0.06	0.01	1				
1160	0.36	-0.20	-0.46	0.72	-0.16	-0.33	-0.33	-0.02	0.08	0.80	0.16	0.20	0.14	0.20	-0.11	-0.81	1			
810	0.24	-0.27	-0.40	0.62	-0.18	-0.12	-0.36	-0.04	0.07	0.51	0.02	-0.62	0.01	0.64	-0.20	-0.50	0.59	1		
715	-0.21	-0.22	0.21	-0.12	0.45	-0.08	0.22	-0.27	-0.33	0.17	-0.07	-0.90	-0.39	-0.32	-0.12	-0.21	-0.01	0.49	1	
Match (r>0.45)	--	--	3	5	0	1	1	1	2	2	1	0	0	1	0	0	1	1	--	

*Contributions $r \geq 0.45$ (given in **bold**) were taken into account for the correlation.

407

408

409

410 **Conclusion**

411 Libraries and collections they have are cultural heritages and there are many factors that affect
412 these precious cultural treasures in many negative ways. One of these factors is air pollution
413 related to traffic. In order to investigate the effects of traffic-driven air pollution on cultural
414 heritage environments, it is important to investigate nearby environments by means of various
415 analytical techniques including DRIFTS. By examining samples that can be taken from non-
416 destructive methods from outside, indoor exposures can be understood as a first step of further
417 indoor analyses. The studies conducted in the last two decades that already used the MIR range
418 have demonstrated the potential of DRIFTS is effective in rapid and inexpensive soil analysis.
419 A major advantage of DRIFTS is its capability of reducing the cost and time of the analysis
420 compared to conventional laboratory techniques. In addition, the measurements are very rapid
421 so that a large number of samples can be easily screened. Given that our findings are based on
422 a limited number of the samples, the results from such analyses should consequently be treated
423 with considerable caution. Traffic lights (sudden and intense effects) and continuous traffic
424 flow should be performed and evaluated as further studies. More sampling from heavy traffic-
425 bearing street is a further requirement. Abundance of embedded mineral fragments in urban
426 topsoil layers could give more information.

427 Providing appropriate comfort conditions (clean, thermal and non-humid) in the
428 environments where collections and cultural heritage assets exist, identifying all hazards and
429 taking precautions for them (appropriate storage, ventilation, etc.) are supportive part to the
430 studies (Kuzucuoğlu, 2017) similar to our effort. Many projects such as the MEMORI (The
431 MEMORI Project, 2010) have been carried out on this subject at the international level. In order
432 to understand the effects of air quality in indoor environments, firstly, the air quality around the
433 historical structures must be measured, analyzed and evaluated. Non-destructive analysis based
434 on soil analysis in the vicinity of these structures has been the scope of this study.

435 **References**

- 436 Bashagaluke, J., Nshobole, N., Fataki, D., Mochoge, B., Mugwe, J., and Walangululu, J.W.,
437 2015. Application of infrared technique in soil properties' characterization in South
438 Kivu province of DR Congo. *African Journal of Food Science and Technology* 6 (2),
439 58-67.
- 440 Bellamy, L.J., 1975. *The Infra-red spectra of complex molecules*; Chapman and Hall: London,
441 p 433.
- 442 Billes, F., Pataki, H., Unsalan, O., Mikosch, H., Vajna, B., Marosi, G., 2012. Solvent effect on
443 the vibrational spectra of Carvedilol. *Spectrochim. Acta Part A: Mol. and Biomol. Spec.*
444 95, 148-164.
- 445 Bishop, J.L., Koeberl, C., Kralik, C., Fröschl, H., Englert, P.A., Andersen, D.W., Pieters, C.
446 M., Wharton, R.A., 1996. *Geochim. Cosmochim. Acta.* 60 (5), 765-785.
- 447 Blanch, A.J., Quinton, J.S., Lenehan, C.E., Pring, A., 2008. The crystal chemistry of Al-bearing
448 goethites: an infrared spectroscopic study. *Mineral. Mag.* 72, 1043–1056.
- 449 Calderon, F.J., Mikha, M.M., Vigil, M.F., Nielsen, D.C., Benjamin, J.G., and Reeves, J.B.,
450 2011. Diffuse-Reflectance Mid-infrared spectral properties of soils under alternative
451 crop rotations in a semi-arid climate. *Comm. in Soil Sci. and Plant Analysis* 42 (17),
452 2143-2159.
- 453 Cannane, N. Oumabady Alisa, Rajendran, M. Selvaraju, R., 2013. FT-IR spectral studies on
454 polluted soils from industrial area at Karaikal Puducherry State, South India.
455 *Spectrochim. Acta Part A: Mol. and Biomol. Spec.*, 110, 46-54.
- 456 Candeias, C., Vicente, E., Tome, M., Rocha, F., Avila, P., Alves, C., 2020. Geochemical,
457 mineralogical and morphological characterisation of road dust and associated health
458 risks. *Int. J. Environ. Res. Public Health* 17 (5).

459 Capriel, P., 1997. Hydrophobicity of organic matter in arable soils: influence of management.
460 Eur. J. Soil Sci. 48 (3), 457-462.

461 Capriel, P., Beck, T., Borchert, H., Gronholz, J., Zachmann, G., 1995. Hydrophobicity of the
462 Organic-Matter in Arable Soils. Soil Biology & Biochemistry 27 (11), 1453-1458.

463 Cases, J.M., Liétard, O., Yvon, J., Delon, J.F., 1982. Étude des propriétés cristallographiques,
464 morphologiques, superficielles de kaolinites désordonnées. Bull. de Minéralogie 105
465 (5), 439-455.

466 Delineau, T., Allard, T., Muller, J.-P., Barres, O., Yvon, J., Cases, J.-M., 1994. FTIR reflectance
467 vs. EPR studies of structural iron in kaolinites. Clays and Clay Minerals 42 (3), 308-
468 320.

469 Dick, D.P., Santos, J.H.Z., Ferranti, E.M., 2003. Chemical characterization and infrared
470 spectroscopy of soil organic matter from two southern Brazilian soils. Revista Brasileira
471 De Ciencia Do Solo 27 (1), 29-39.

472 Downey, G., Briandet, R., Wilson, R.H., Kemsley, E.K., 1997. Near- and mid-infrared
473 spectroscopies in food authentication: Coffee varietal identification. J. of Agricultural
474 and Food Chem. 45 (11), 4357-4361.

475 Ellerbrock, R.H., Gerke, H.H., Bohm, C., 2009. In situ DRIFT characterization of organic
476 matter composition on soil structural surfaces. Soil Science Society of America Journal
477 73 (2), 531-540.

478 Erdogdu, Y. Dereli, Ö, Sajan, D., Joseph, L., Unsalan, O., Gulluoglu, M.T., 2012. Vibrational
479 (FT-IR and FT-Raman) spectral investigation of 7-aminoflavone with density functional
480 theoretical simulations. Mol. Sim., 38 (4) 315-325.

481 Forrester, S., Janik, L., McLaughlin, M., 2010. An infrared spectroscopic test for total
482 petroleum hydrocarbon (TPH) contamination in soils, pp. 13-16. International Union of

483 Soil Sciences (IUSS), c/o Institut für Bodenforschung, Universität für Bodenkultur,
484 Wien.

485 Forrester, S.T., Janik, L.J., McLaughlin M.J., Soriano-Disla, J.M., Stewart, R., Dearman, B.,
486 2013. Total petroleum hydrocarbon concentration prediction in soils using diffuse
487 reflectance infrared spectroscopy. *Soil Science Society of America Journal* 77 (2), 450-
488 460.

489 Gonzalez-Grijalva, B., Meza-Figueroa, D., Romero, F.M., Robles-Morua, A., Meza-
490 Montenegro, M., Garcia-Rico, L., Ochoa-Contreras, R., 2019. The role of soil
491 mineralogy on oral bioaccessibility of lead: Implications for land use and risk
492 assessment. *Sci. Total Environ.* 657, 1468-1479.

493 Hobley, E., Willgoose, G.R., Frisia, S., Jacobsen, G., 2014. Vertical distribution of charcoal in
494 a sandy soil: evidence from DRIFT spectra and field emission scanning electron
495 microscopy. *Eur. J. of Soil Sci.* 65 (5), 751-762.

496 Horta, A., Malone, B., Stockmann, U., Minasny, B., Bishop, T.F.A., McBratney, A.B.,
497 Pallasser, R., Pozza, L., 2015. Potential of integrated field spectroscopy and spatial
498 analysis for enhanced assessment of soil contamination: A prospective review.
499 *Geoderma* 241-242, 180-209.

500 Íslam, N., Rabha, S., Silva, Luis. F. O., Saikia, Binoy, K., 2019. Air quality and PM₁₀-associated
501 poly-aromatic hydrocarbons around the railway traffic area: statistical and air mass
502 trajectory approaches. *Environ. Geochem. Health.* 41, 2309-2053.

503 Janik, L.J., Merry, R.H., Skjemstad, J.O., 1998. Can mid infrared diffuse reflectance analysis
504 replace soil extractions?. *Australian Journal of Experimental Agriculture* 38 (7), 681-
505 696.

506 Jiang, H.-H., Cai, L.-M., Wen, H.-H., Hu, G.-C., Chen, L.-G., Luo, J., 2020a. An integrated
507 approach to quantifying ecological and human health risks from different sources of soil
508 heavy metals. *Sci. of The Total Environ.* 701, 134466.

509 Jiang, H.-H., Cai, L.-M., Wen, H.-H., Luo, J., 2020b. Characterizing pollution and source
510 identification of heavy metals in soils using geochemical baseline and PMF approach.
511 *Sci. Rep.* 10 (1), 6460.

512 Kaiser, K., Guggenberger, G., Haumaier, L., Zech, W., 1997. Dissolved organic matter sorption
513 on subsoils and minerals studied by C-13-NMR and DRIFT spectroscopy. *Eur. J. of Soil*
514 *Sci.* 48 (2), 301-310.

515 Kaluderović, Lazar M., Tomić, Zorica P., Ašanin, Darko P., Đurović-Pejčev, Rada D.,
516 Kresović, Branka J., 2018. Examination of the influence of phenyltrimethylammonium
517 chloride (PTMA) concentration on acetochlor adsorption by modified montmorillonite.
518 *J. of Environ. Sci. and Health, Part B.* 53 (8), 503-509.

519 Kemsley, E.K., Holland, J.K., Defernez, M., Wilson, R.H., 1996. Detection of adulteration of
520 raspberry purees using infrared spectroscopy and chemometrics. *J. of Agricultural and*
521 *Food Chemistry* 44 (12), 3864-3870.

522 Kim, S.-O., Kim, J.-J., Yun, S.-T., Kim, K.-W., 2003. Numerical and experimental studies on
523 cadmium (II) transport in kaolinite clay under electrical fields. *Water, Air, and Soil*
524 *Pollution* 150 (1), 135-162.

525 Koretsky, Carla M., Sverjensky, Dimitri A., Salisbury John W., D'Aria, Dana M., 1997.
526 Detection of surface hydroxyl species on quartz, γ -alumina, and feldspars using diffuse
527 reflectance infrared spectroscopy. *Geochim. et Cosmochim. Acta*, 61 (11), 2193-2210.

528 Kubelka, P., Munk, F., 1931. Ein beitrag zur optik der farbanstriche. *Z. Techn. Phys.* 12, 593-
529 601.

530 Kuzucuoğlu, A., 2017. Preventive conservation in cultural heritage case study: MEMORI
531 survey, Journal of Art, Istanbul University,
532 <https://dergipark.org.tr/tr/pub/iuarts/issue/47768/603431>

533 Kuzucuoğlu, A.H., Kiraz, N.M., Unsalan, O., Taşdemir, İ., 2015. A documentation proposal
534 for manuscripts in libraries A case study: İstanbul University Faculty of Letters Rare
535 Books Library. *Bilgi Dünyası* 16 (1), 141-159.

536 Leue, M., Gerke, H.H., Ellerbrock, R.H., 2013. Millimetre-scale distribution of organic matter
537 composition at intact biopore and crack surfaces. *Eur. J. of Soil Sci.* 64 (6), 757-769.

538 Machovic, V., Novak, F., 1998. Diffuse reflectance infrared spectroscopy of soil bitumens from
539 Sumava region. *Chemicke Listy* 92 (2), 151-156.

540 Margenot, A.J., Calderon, F.J., Magrini, K.A., Evans, R.J., 2017. Application of DRIFTS, C-
541 13 NMR, and py-MBMS to Characterize the effects of soil science oxidation assays on
542 soil organic matter composition in a mollic xerofluvent. *Appl. Spec.* 71 (7), 1506-1518.

543 Menges, F., 2020. Spectragryph - optical spectroscopy software, Version 1.2.14, 2020,
544 <http://www.ffmpeg2.de/spectragryph/>.

545 Messerschmidt, R.G., 1985. Complete elimination of specular reflectance in Infrared diffuse
546 reflectance measurements. *Appl. Spec.* 39 (4), 737-739.

547 Mohsenipour, M., Shahid, S., Ebrahimi, K., 2015. Nitrate adsorption on clay kaolin: Batch
548 Tests. *J. of Chemistry* 2015, 397069.

549 Montecchio, D., Francioso, O., Carletti, P., Pizzeghello, D., Chersich, S., Previtali, F., Nardi,
550 S., 2006. Thermal analysis (TG-DTA) and drift spectroscopy applied to investigate the
551 evolution of humic acids in forest soil at different vegetation stages. *J. of Thermal*
552 *Analysis and Calorimetry* 83 (2), 393-399.

553 Muller, J.P., Ildefonse, P., Calas, G., 1990. Paramagnetic defect centers in hydrothermal
554 kaolinite from an altered tuff in the nopal uranium deposit, Chihuahua, Mexico. *Clays
555 and Clay Minerals* 38 (6), 600-608.

556 Muller, J.P., Bocquier, G., 1987. Textural and mineralogical relationships between ferruginous
557 nodules and surrounding clayey matrices in a laterite from Cameroon, in: Schulz, L.G.,
558 van Olphen H., Mumpton, F.A. Eds.), *Proceedings of the International Clay Conference*,
559 Bloomington, Indiana, pp. 186-194.

560 Ng, W., P. Malone, B., Minasny, B., 2017. Rapid assessment of petroleum-contaminated soils
561 with infrared spectroscopy. *Geoderma* 289, 150-160.

562 Nguyen, T.T., Janik, L.J., Raupach, M., 1991. Diffuse reflectance infrared Fourier-Transform
563 (Drift) spectroscopy in soil studies. *Australian J. of Soil Res.* 29 (1), 49-67.

564 Niemeyer, J., Chen, Y., Bollag, J.M., 1992. Characterization of humic acids, composts, and
565 peat by diffuse reflectance Fourier-Transform infrared-spectroscopy. *Soil Science
566 Society of America Journal* 56 (1), 135-140.

567 Parikh, Sanjai J., Goyne, Keith W., Margenot, Andrew J., Mukome, Fungai N. D., Calderón,
568 Francisco J., 2014. Soil chemical insights provided through vibrational spectroscopy.
569 Publications from USDA-ARS / UNL Faculty. Paper 1471.

570 Pieters, C.M., Englert, P.A.J., 1993. Eds. *Remote geochemical analysis: Elemental and
571 mineralogical composition*; Cambridge University Press: Cambridge, p 594.

572 Reeves, J.B., 2012. Mid-Infrared spectroscopy of biochars and spectral similarities to coal and
573 kerogens: What are the implications? *Appl. Spect.* 66 (6), 689-695.

574 Reeves, J., McCarty, G., Mimmo, T., 2002. The potential of diffuse reflectance spectroscopy
575 for the determination of carbon inventories in soils. *Environ. Pollution* 116, S277-S284.

576 Reeves, J.B., McCarty, G.W., Reeves, V.B., 2001. Mid-infrared diffuse reflectance
577 spectroscopy for the quantitative analysis of agricultural soils. *J. of Agricultural and*
578 *Food Chem.* 49 (2), 766-772.

579 Reeves, J.B., 2001a. Near- versus mid-infrared diffuse reflectance spectroscopy for
580 determination of minerals in dried poultry manure. *Poultry Science* 80 (10), 1437-1443.

581 Reeves, J.B., 2001b. Near-infrared diffuse reflectance spectroscopy for the analysis of poultry
582 manures. *Journal of Agricultural and Food Chemistry* 49 (5), 2193-2197.

583 Reeves, J.B., 1994a. Influence of pH, ionic-strength, and physical state on the near-infrared
584 spectra of model compounds. *J. of Aoac International* 77 (4), 814-820.

585 Reeves, J.B., 1994b. Solid-state matrix effects on the near-infrared (NIR) spectra of sugars.
586 *Abstracts of Papers of the American Chemical Society* 208, 4-Carb.

587 Russell, J.D., 1987. Infrared methods, a handbook of determinative methods in clay mineralogy,
588 edited by Wilson. Chapman and Hall. New York., pp. 133-173. Blackie and Son,
589 London.

590 Schwertmann, U., Taylor, R.M., 1989. Iron oxides. In: *Minerals in Soil Environments* (eds
591 Dixon, J.B. and Weed, S.B.), pp. 379-438. Soil Science Society of America, Madison,
592 WI.

593 Soda, R., 1961. Infrared absorption spectra of quartz and some other silica modifications. *Bull.*
594 *of the Chem. Soc. of Japan* 34 (10), 1491-1495.

595 The MEMORI project., 2010. Measurement, Effect assessment and Mitigation of Pollutant
596 Impact on Movable Cultural Assets. Innovative Research for Market Transfer", is
597 implemented within the EU 7th Framework Programme.
598 <http://www.memori.fraunhofer.de/>

599 Unsalan, O., Kuzucuoglu, A.H., Cakir, C., Kaygisiz, E., 2017. One pilot application of mobile
600 Raman spectroscopy and information technologies for cultural heritage inventory
601 studies. *J. of Cult. Her.* 25, 94-100.

602 Unsalan, O., Kuzucuoglu, A.H., 2016. Effects of hazardous pollutants on the walls of Valence
603 Aqueduct (Istanbul) by Raman spectroscopy, SEM-EDX and Geographical Information
604 System. *Spectrochim. Acta Part A: Mol. and Biomol. Spec.* 152, 572-576.

605 Unsalan, O., Kus, N., Jarmelo, S., Fausto, R., 2015. Trans- and cis-stilbene isolated in cryogenic
606 argon and xenon matrices. *Spectrochim. Acta Part A: Mol. and Biomol. Spec.* 136, 81-
607 94.

608 Unsalan, O., Sert, Y., Ari, H., Simão, A., Yilmaz, A., Boyukata, M., Bolukbasi, O., Bolelli, K.,
609 Yalcin, I., 2014. Micro-Raman, Mid-IR, Far-IR and DFT studies on 2-[4-(4-
610 Fluorobenzamido)phenyl]benzothiazole *Spectrochim. Acta Part A: Mol. and Biomol.*
611 *Spec.* 125, 414-421.

612 Unsalan, O., Yilmaz, A. Bolukbasi, O. Ozturk, B., Esenoglu, H.H., Ildiz, G.O., Ornek, C.Y.,
613 2012. Micro-Raman, FTIR, SEM-EDX and structural analysis of the Çanakkale
614 meteorite. *Spectrochim. Acta Part A: Mol. and Biomol. Spec.* 92, 250-255.

615 van der Marel H. W. and Beutelspacher H., 1976. *Atlas of Infrared spectroscopy of clay minerals*
616 *and their admixtures.* Elsevier, Amsterdam.

617 Verma, S.K., Deb, M.K., Bajpai, S., Suzuki, Y., Sinha, S.K., Gong, Y., 2007. A simple diffuse
618 reflectance Fourier transform infrared spectroscopic determination of sulfur dioxide in
619 ambient air using potassium tetrachloromercurate as the absorbing reagent. *J. AOAC*
620 *Int.* 90 (4), 1180-90.

621 Verma, S.K., Deb, M.K., 2007a. Direct and rapid determination of sulphate in environmental
622 samples with diffuse reflectance Fourier transform infrared spectroscopy using KBr
623 substrate. *Talanta* 71 (4), 1546-52.

624 Verma, S.K., Deb, M.K., 2007b. Nondestructive and rapid determination of nitrate in soil, dry
625 deposits and aerosol samples using KBr-matrix with diffuse reflectance Fourier
626 transform infrared spectroscopy (DRIFTS). *Anal. Chim. Acta* 582 (2), 382-9.

627 Wang, C., Li, W., Guo, M., Ji, J., 2017. Ecological risk assessment on heavy metals in soils:
628 Use of soil diffuse reflectance mid-infrared Fourier-transform spectroscopy. *Sci. Rep.*
629 7, 40709.

630 Woelki, G., Friedrich, S., Hanschmann, G., Salzer, R., 1997. HPLC fractionation and structural
631 dynamics of humic acids. *Fresenius J. Anal. Chem.* 357, 548-552.

632 Zeine, C., Grobe, J., 1997. Diffuse reflectance infrared Fourier transform (DRIFT)
633 spectroscopy in the preservation of historical monuments: Studies on salt migration.
634 *Microchim. Acta* 125 (1-4), 279-282.

635

636